

Evolution of phonon anharmonicity in Se-doped Sb_2Te_3 thermoelectrics

Diptasikha Das,¹ Subarna Das,¹ P. Singha,¹ K. Malik,² A. K. Deb,³ A. Bhattacharyya,⁴ V. A. Kulbachinskii,⁵ Raktima Basu,⁶ Sandip Dhara,⁶ S. Bandyopadhyay,^{1,7,*} and Aritra Banerjee^{1,7,*}

¹Department of Physics, University of Calcutta, 92 A P C Road, Kolkata 700 009, India

²Department of Physics, Vidyasagar Evening College, 39 Sankar Ghosh Lane, Kolkata 700 006, India

³Department of Physics, Raiganj University, Uttar Dinajpur, West Bengal 733 134, India

⁴Saha Institute of Nuclear Physics, 1/AF Bidhannagar, Kolkata 700 064, India

⁵Department of Low Temperature Physics and Superconductivity, Physics Faculty,

M.V. Lomonosov Moscow State University - 119991, Moscow, Russia

⁶Surface and Nanoscience Division, Indira Gandhi Centre for Atomic Research, Homi Bhabha National Institute, Kalpakkam 603 102, India

⁷Center for Research in Nanoscience and Nanotechnology, University of Calcutta, JD-2, Sector-III, Saltlake, Kolkata 700 106, India

(Received 31 May 2017; revised manuscript received 9 August 2017; published 29 August 2017)

The phonon anharmonicity in Se-doped Sb_2Te_3 system is probed both macroscopically and microscopically using temperature-dependent synchrotron powder diffraction, Raman spectroscopic studies, and heat-capacity measurements. Gruneisen parameter (γ_G) is calculated to explain anharmonicity in the polycrystalline $\text{Sb}_2\text{Te}_{3-x}\text{Se}_x$ samples. The thermal variation of structural parameters, structural anisotropy, Debye temperature, velocity of sound, and isothermal compressibility of $\text{Sb}_2\text{Te}_{3-x}\text{Se}_x$ at room temperature are estimated. Analysis revealed that structural anisotropy and phonon anharmonicity are correlated. Further, lattice thermal conductivities (κ_L), evaluated in the Umklapp scattering limit in terms of γ_G , indicate that the phonon anharmonicity increasing with Se(x) content reduces κ_L . A plausible explanation is provided on the basis of Se-doped softening of transverse optical phonon mode.

DOI: [10.1103/PhysRevB.96.064116](https://doi.org/10.1103/PhysRevB.96.064116)

I. INTRODUCTION

Sb_2Te_3 and related binary pnictide chalcogenides are well known for their potential thermoelectric (TE) applications [1]. Furthermore, Sb_2Te_3 is a three-dimensional topological insulator [2]. Topological insulator behavior is also verified in Sb_2Se_3 , $\text{Sb}_2\text{Te}_2\text{Se}$, Bi_2Se_3 , and related metal chalcogenides, where Se is isoelectronic to Te [2–6]. Sb_2Te_3 is p -type in nature, where antisite defects play a major role. The concentration of holes in the system decreases with tuning of compositions from Sb_2Te_3 to $\text{Sb}_2\text{Te}_2\text{Se}$. It is evidenced that around the composition $\text{Sb}_2\text{Te}_2\text{Se}$, the Se/Te sublattice is expected to be ordered with an almost complete compensation of donor and acceptor impurities [7–9]. However, although the topological insulating properties of Se-doped metal chalcogenides are explored well, TE properties of them are yet to be studied extensively [4,7,9]. Low thermal conductivity (κ) is favorable for good thermoelectric performance. Sb_2Te_3 -based layered binary compounds with rhombohedral crystal structure ($R\bar{3}m$) are particularly interesting with high ZT values around room temperature, in parts thanks to its low lattice thermal conductivities, $\kappa_L = 2.4 \text{ Wm}^{-1}\text{K}^{-1}$ at 300 K [10]. Several factors, i.e., soft bonds, heavy atomic masses, and strong anharmonicity, contribute to this low κ_L [10–12].

Ternary mixed-crystal $\text{Sb}_2\text{Te}_{3-x}\text{Se}_x$ possesses heavy atomic mass. The layered structure offers soft bond in Sb_2Te_3 -based system. Sb_2Te_3 exhibits a lattice structure with each layer comprising quintuple [Te(I)-Sb-Te(II)-Sb-Te(I)] stacks (QLs). Three such QLs form the Sb_2Te_3 unit cell, where QLs are interconnected by weak van der Waals force. In

$\text{Sb}_2\text{Te}_{3-x}\text{Se}_x$ system, Se replaces Te atoms. Te(I)/Se(I) and Te(II)/Se(II) denote two types of differently bonded Te(Se) atoms. The weak van der Waals binding between the -[Te(I) . . . Te(I)]- layers leads to the easy cleavage of Sb_2Te_3 systems perpendicular to the c axis. The observed unit-cell elongation $c/a \sim 7$ is indicative of a large structural anisotropy [13]. This highly anisotropic nature results in a compressed Brillouin zone and gives rise to transport and elastic anisotropy [1,14]. However, the effect of this anisotropy on the phonon dynamics and phonon anharmonicity remains unexplored, to the best of our knowledge.

Understanding the lattice dynamics, corresponding phonon anharmonicity, and its relation with low κ_L is critical to the development of better TE property. Systems with intrinsically strong anharmonicity in their lattice potential help to decouple phonon and electron transport. Phonon anharmonicity in Te- and Se-based TE systems, viz., SnSe, SnTe, PbTe, is extensively studied [10–12,15–18]. Raman spectroscopic studies and pump-probe experiments depict the importance of phonons in modulating fundamental scattering processes for the Bi_2S_3 and Sb_2S_3 system [19,20]. Large anharmonic effect and thermal expansion anisotropy of Sb_2S_3 have been recently reported by Gan *et al.* [21]. Very recently, Tian *et al.* [5] reported the evolution of anharmonicity in various phonon modes in $\text{Bi}_2\text{Te}_{3-x}\text{Se}_x$. On the other hand, there are very limited efforts to elucidate the role of phonon anharmonicity in Sb_2Te_3 -based system [1,22–24]. Temperature-dependent Raman spectra and thermal expansion parameters of Sb_2Te_3 crystals are analyzed considering the anharmonic decay of optical phonons and the Gruneisen parameter (γ_G), which points out the role of higher-order anharmonic effects in the high-temperature regime [22,23]. A similar feature of analyzing the temperature dependence of phonon frequency in Sb_2Te_3 system with the help of a three-phonon coupling model

*Author to whom correspondence should be addressed: arbphy@caluniv.ac.in

was recently documented by Tian *et al.* [24]. However, Bessas *et al.* [1] investigated the lattice dynamics in Sb_2Te_3 both microscopically and macroscopically and demonstrated that the observed low κ_L could not be explained by anharmonicity alone. It is thus needless to say that in-depth understanding of lattice dynamics and its relation with low κ_L for Sb_2Te_3 -based systems is still elusive in nature. Most importantly, there are hardly any reports to date to understand the effect of doping on the phonon anharmonicity of Sb_2Te_3 -based TE material.

We herein report both the microscopic characterization of polycrystalline ternary mixed-crystal $\text{Sb}_2\text{Te}_{3-x}\text{Se}_x$ samples by temperature-dependent synchrotron radiation diffraction and Raman spectroscopic measurements, as well as macroscopic characterization based on heat-capacity (C_p) measurements. The combination of these measurements provides a detailed view of the phonon dynamics and anharmonicity. κ_L is evaluated in terms of γ_G . Temperature dependence of vibrational phonon mode is analyzed considering the anharmonic decay of optical phonons and the material thermal expansion. The mode Gruneisen parameters ($\overline{\gamma_G}$) are calculated to illustrate the anharmonicity of the vibrational mode and it is demonstrated that the anharmonic contribution in lattice thermal expansion is directly correlated with γ_G . In addition, structural anisotropy of the synthesized samples is evaluated from powder-diffraction data and its correlation with phonon anharmonicity is obtained. The speed of sound in $\text{Sb}_2\text{Te}_{3-x}\text{Se}_x$ samples is estimated using microscopic parameters. Finally, the role of Se(x) content on low κ_L , lattice anharmonicity, and speed of sound is derived and their correlations are established.

II. EXPERIMENTS

Polycrystalline $\text{Sb}_2\text{Te}_{3-x}\text{Se}_x$ ($x = 0.2, 0.6, 1.0$) samples were synthesized by the solid-state reaction method [7,25]. Stoichiometric amounts of Sb, Te, and Se (each of purity 99.999%; Alfa Aesar, UK) were sealed in a quartz tube under pressure of 10^{-3} Pa to avoid oxidation. Vacuum-sealed quartz ampoules were initially annealed at temperature of 1123 K for 24 h and cooled down to 893 K at the rate 5 K/h. It was then sintered at 893 K for 96 h to homogenize the samples, followed by quenching in liquid nitrogen.

Low-temperature powder-diffraction experiments were carried out using the synchrotron radiation facility at Indian beam line BL-18B, Photon Factory, KEK, Japan. The polycrystalline powder samples were illuminated by a monochromatic x-ray beam with wavelength $\lambda = 0.0799 \pm 10^{-4}$ nm. The x-ray diffraction (XRD) measurement was performed in $4^\circ \leq 2\theta \leq 40^\circ$ range. The data for powder-diffraction experiments were collected during heating. For $\text{Sb}_2\text{Te}_{2.8}\text{Se}_{0.2}$ (i.e., $x = 0.2$) sample, the low-temperature XRD data were collected with a 100 K 2D Pilatus detector and were converted using IMAGEJ software. A point detector (Cyberstar X2000) was employed for data collection of $\text{Sb}_2\text{Te}_{2.4}\text{Se}_{0.6}$ and $\text{Sb}_2\text{Te}_2\text{Se}$ samples and room-temperature data of $\text{Sb}_2\text{Te}_{2.8}\text{Se}_{0.2}$. The instrumental profile was refined using NIST Si 640d as an external standard. The synchrotron powder-diffraction data were analyzed using the Rietveld refinement technique with the software MAUD (Materials Analysis Using Diffraction) [26]. The refinement was carried out using both atomic position and substitution, i.e., site occupancy. The space group $R\bar{3}m$ and

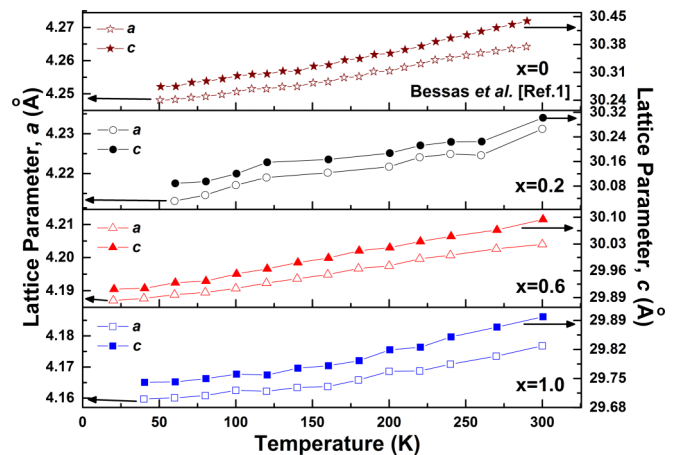


FIG. 1. Lattice constants a and c of $\text{Sb}_2\text{Te}_{3-x}\text{Se}_x$ ($x = 0, 0.2, 0.6, 1.0$) samples as a function of temperature. For comparison, we have co-plotted thermal variation of lattice parameters of Sb_2Te_3 , as obtained by Bessas *et al.* [1]. Estimated errors in the refined lattice parameters are within the size of the data points and are provided in Fig. SM1 of the Supplemental Material [13].

point group D_{3d} with a hexagonal coordinate system were used for refinement. Raman spectroscopic (model: inVia; make: Renishaw, UK) studies between the temperature range of 80 to 300 K, in a thermoelectric heating and cooling function assisted Linkam (THMS600) stage, were performed in the range of $50\text{--}400\text{ cm}^{-1}$ with 514.5 nm of Ar^+ laser excitation using small flakes of respective samples. A submicrometer focusing diameter was used with a long working distance $50 \times$ objective having a numerical aperture of 0.35. An 1800 gr/mm grating was used for monochromatization with a thermoelectric cooled charge-coupled device as detector in the backscattering configuration. Thermal variation of C_p was measured in the temperature range of $4\text{--}300\text{ K}$ by the semiadiabatic heat-pulse method.

III. RESULTS AND DISCUSSION

Thermal variation of structural parameters of the $\text{Sb}_2\text{Te}_{3-x}\text{Se}_x$ ($x = 0.2, 0.6, 1.0$) samples is extracted using Rietveld refinement. The diffraction patterns after refinement [13], along with the refined parameters, are presented in the Supplemental Material [13]. Sharp peaks are observed, as indicative of the polycrystalline nature of the samples. All the peaks are indexed to rhombohedral crystal structure ($R\bar{3}m$), with no signature of impurity phases. The XRD data further indicate that all the Se-doped Sb_2Te_3 samples retain their A7-type rhombohedral phase until the lowest measured temperature (20 K). Temperature-dependent refined lattice parameters of the synthesized samples are presented in Fig. 1. Both the lattice parameters a and c decrease with decreasing temperature. The refined lattice parameters indicate that the $\text{Sb}_2\text{Te}_{3-x}\text{Se}_x$ samples possess structural anisotropy with large unit-cell elongation, $c/a \sim 7$ [13]. The thermal variation of c/a ratio, as plotted in Fig. 2, depicts that the structural anisotropy is temperature dependent and increases with increasing temperature. Further, at a particular

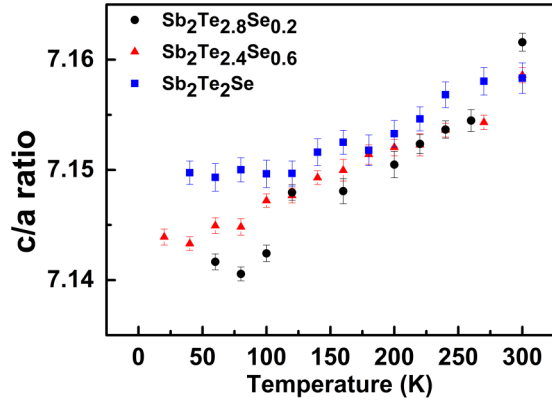


FIG. 2. Variation of the c/a ratio with temperature for $\text{Sb}_2\text{Te}_{3-x}\text{Se}_x$ ($0.2 \leq x \leq 1.0$) samples.

temperature the observed structural anisotropy increases with increasing Se concentration.

The measured C_p between 4 and 300 K of $\text{Sb}_2\text{Te}_{3-x}\text{Se}_x$ samples are plotted in Fig. 3. For all the $\text{Sb}_2\text{Te}_{3-x}\text{Se}_x$ ($x = 0.2, 0.6$, and 1.0) samples reported here, the measured $C_p(T)$ deviates linearly from the Dulong-Petit value, $124.5 \text{ Jmol}^{-1}\text{K}^{-1}$ between 200 and 300 K (Table I). The deviation between the measured C_p and theoretical value of specific heat at constant volume C_v in pristine Sb_2Te_3 was previously reported, with the deviation between C_p and C_v ($\Delta C_p = C_p - C_v$) per unit K being around $0.04 \text{ Jmol}^{-1}\text{K}^{-2}$ [1,27]. This is in agreement with the $\Delta C_p/K$ values obtained for the present $\text{Sb}_2\text{Te}_{3-x}\text{Se}_x$ system at 300 K (Table I). Table I

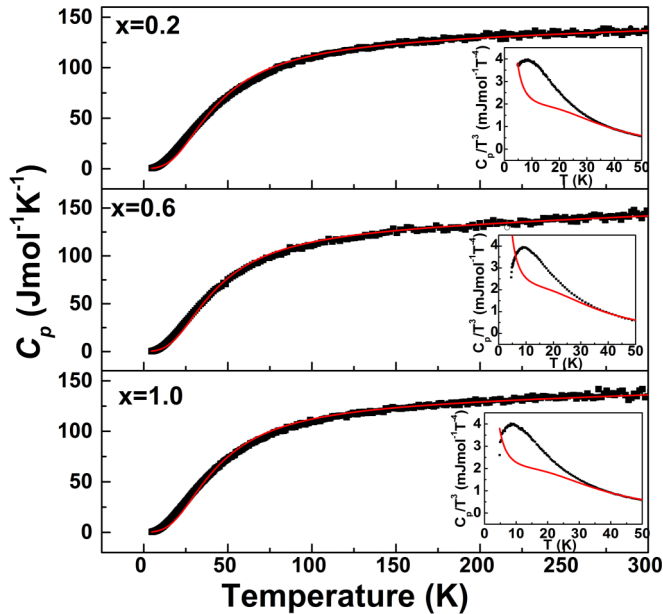


FIG. 3. Thermal variation of specific heat at constant pressure C_p of the $\text{Sb}_2\text{Te}_{3-x}\text{Se}_x$ ($x = 0.2, 0.6$, and 1.0) samples. The red solid lines represents the best fit of C_p data to the Debye model: $C_p = \gamma T + 9R(T/\theta_D)^3 \int_0^{\theta_D/T} [x^4 e^x / (e^x - 1)^2] dx$. (Inset) C_p/T^3 vs T plot of the samples reveals the deviation from the Debye model below 30 K. The typical errors in C_p values are less than 2% and are within the size of the data points.

TABLE I. Thermodynamical parameters: Deviation of measured C_p value from Dulong-Petit law (ΔC_p) at 300 K, ΔC_p per Kelvin ($\Delta C_p/K$), isothermal compressibility (K_T), Debye temperature (θ_D), extracted from specific heat ($C_p - T$) measurements for different Se-doped Sb_2Te_3 samples.

Sample	ΔC_p ($\text{Jmol}^{-1}\text{K}^{-1}$)	$\Delta C_p/K$ ($\text{Jmol}^{-1}\text{K}^{-2}$)	K_T (Mbar^{-1})	θ_D (K)
$\text{Sb}_2\text{Te}_{2.8}\text{Se}_{0.2}$	12.5 ± 1.5	0.042 ± 0.005	4.10 ± 0.49	172
$\text{Sb}_2\text{Te}_{2.4}\text{Se}_{0.6}$	16.5 ± 1.9	0.055 ± 0.006	2.70 ± 0.31	174
$\text{Sb}_2\text{Te}_2\text{Se}$	18.5 ± 2.2	0.062 ± 0.007	2.95 ± 0.35	177

further depicts that ΔC_p increases with increasing $\text{Se}(x)$. The effect of anharmonicity to specific heat at around room temperature is expressed by the formula [28]

$$C_p - C_v = \frac{\beta^2 V}{K_T} T, \quad (1)$$

where K_T is the isothermal compressibility and $\beta (= 2\alpha_c + \alpha_a)$ is the volumetric thermal expansion coefficient. The estimated K_T , based on our C_p measurement, varies between 2.7 and 4 Mbar^{-1} (Table I) for the present $\text{Sb}_2\text{Te}_{3-x}\text{Se}_x$ samples and is in excellent agreement with the K_T data reported for Sb_2Te_3 [29]. Thus, the observed ΔC_p for the Se-doped Sb_2Te_3 have an anharmonic origin, which increases with Se content. Further, the $C_p(T)$ data are fitted with the Debye model, which accounts for the collective motion of phonons throughout the $\text{Sb}_2\text{Te}_{3-x}\text{Se}_x$ crystals [30]:

$$C_p = \gamma T + 9R \left(\frac{T}{\theta_D} \right)^3 \int_0^{\theta_D/T} \frac{x^4 e^x}{(e^x - 1)^2} dx, \quad (2)$$

where γT represents electronic contribution, γ is the Sommerfeld coefficient, and $x = hv/k_B T$, $\theta_D = hv_D/k_B$, where θ_D is the Debye temperature, v_D is the Debye frequency, and R is the gas constant. The solid lines in Fig. 3 demonstrate that the $C_p(T)$ data of $\text{Sb}_2\text{Te}_{3-x}\text{Se}_x$ samples can be described fairly well by the Debye model [Eq. (2)]. The θ_D values, estimated for the Se-doped Sb_2Te_3 samples (Table I), agree well within the range with those reported in literature for Sb_2Te_3 [31]. However, close observation reveals that there is a significant difference in measured and calculated C_p values at the low-temperature regime (below 30 K). An earlier report speculates it to be a Schottky-like contribution [1]. Schottky anomalies in $C_p(T)$ data are reported in other different systems [32,33]. Defect plays a significant role in Sb_2Te_3 -based TE materials. Moreover, in conjunction with the observations of Saint-Paul *et al.* [34] and Bessas *et al.* [1], it is quite justified to assume that the presence of defects gives rise to Schottky anomaly in $C_p(T)$ of $\text{Sb}_2\text{Te}_{3-x}\text{Se}_x$.

Thermal expansion coefficient (α_L) is an important tool for device designing and engineering. Strain induced due to thermal expansion or contraction can cause the deformation of the device and may affect its phonon dynamics. Thus, the knowledge of α_L is necessary for the understanding of the performance of a TE material [22]. The thermal expansion coefficients, α_L 's, i.e., α_a and α_c of the $\text{Sb}_2\text{Te}_{3-x}\text{Se}_x$ samples, are obtained from the derivative $\alpha_a = [d(\ln a)/dT]$ of the

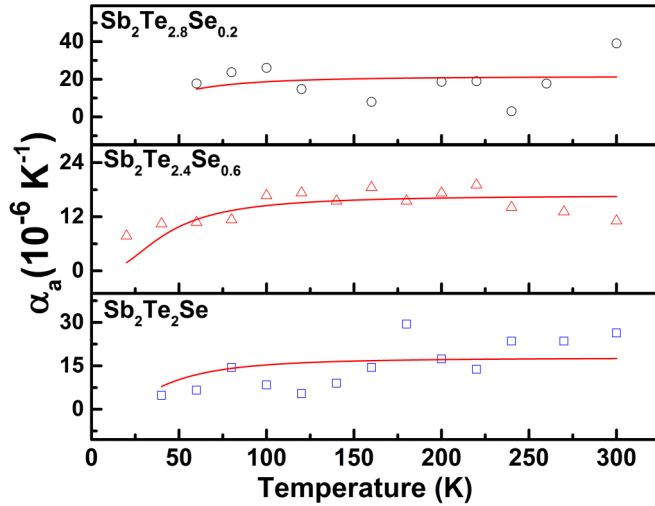


FIG. 4. Temperature dependence of the coefficient of linear thermal expansion α_a for the Se-doped Sb_2Te_3 samples. Errors associated with α_a are within the size of the data points.

lattice parameter a and the corresponding expression for c and plotted in Figs. 4 and 5, respectively. The estimated α_a and α_c values are in excellent agreement with the previously reported values for pristine Sb_2Te_3 samples [22,31]. In order to understand the temperature dependence of α_a and α_c , the Gruneisen relation is employed [1,22]:

$$C_p \gamma_G = B\beta, \quad (3)$$

where B is the bulk modulus. Since γ_G and B are almost temperature independent, it is quite justified to assume that α_L 's, i.e., α_a and α_c , should have the same temperature dependence as the specific heat. An attempt is made to apply the Debye model to fit the temperature dependence of α_L , i.e., $\alpha_L(T)$ data:

$$\alpha_L(T) = \alpha_0 \left(\frac{T}{\theta_D} \right)^3 \int_0^{\theta_D/T} \frac{x^4 e^x}{(e^x - 1)^2} dx, \quad (4)$$

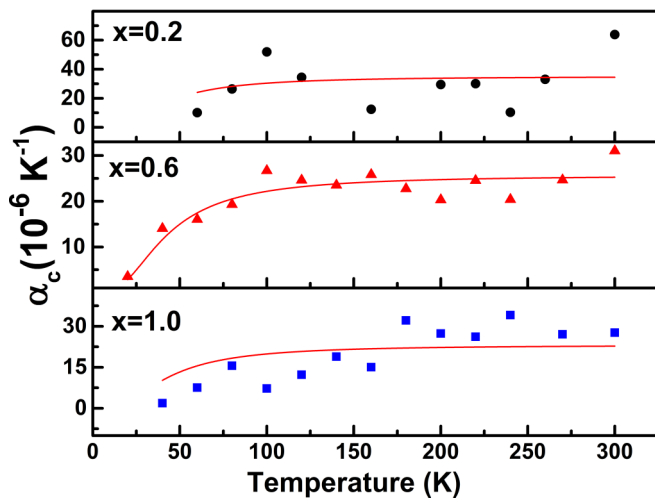


FIG. 5. Variation of linear thermal expansion coefficient α_c with temperature for the synthesized $\text{Sb}_2\text{Te}_{3-x}\text{Se}_x$ samples. The errors in α_c are within the size of the data points.

where α_0 is a temperature-independent fitting parameter. Solid lines in Figs. 4 and 5, representing best fits using the Debye model, indicate that estimated $\alpha_L(T)$ value deviates from the Debye model for the entire temperature range of measurement in the synthesized $\text{Sb}_2\text{Te}_{3-x}\text{Se}_x$ samples. In contrast for single-crystalline Sb_2Te_3 topological insulator, $\alpha_L(T)$ is described well by the Debye model from 2 to 290 K, excluding the anomalous region in $\alpha_L(T)$ around 225–236 K [31]. Chen *et al.* [22] also previously reported that for Sb_2Te_3 single crystals, $\alpha_L(T)$ data well agree with the Debye T^3 law at low temperatures, while above 150 K the experimental results deviate from the Debye model [22]. The observed deviation of $\alpha_L(T)$ data from the Debye model is probably due to the presence of higher-order anharmonic effects [22]. The anharmonicity of the bonding forces is characterized by the γ_G . The γ_G is considered as a measure of anharmonicity and is extracted using Eq. (3). Using C_p and β , as estimated for the $\text{Sb}_2\text{Te}_{3-x}\text{Se}_x$ samples at 300 K and the B value ($= 44.8$ GPa) [22] reported for Sb_2Te_3 samples, yields $\gamma_G = 2.39 \pm 0.012, 2.44 \pm 0.012$, and 2.65 ± 0.013 for the $x = 0.2, 0.6$, and 1.0 samples, respectively. Since no B values are reported in the literature for the $\text{Sb}_2\text{Te}_{3-x}\text{Se}_x$ samples, B values of pristine Sb_2Te_3 samples are used for the calculation. It is also quite justified to assume that the bulk modulus does not change significantly for minimal Se doping. In addition, the estimated $\overline{\gamma_G}$ (discussed later) indicates the same value for the Se-doped Sb_2Te_3 samples. The γ_G values in corroboration with the observed deviation of $\alpha_L(T)$ from the Debye model clearly indicate that phonon anharmonicity prevails in Se-doped Sb_2Te_3 samples. In addition, the temperature-dependent structural anisotropy evidenced in the $\text{Sb}_2\text{Te}_{3-x}\text{Se}_x$ samples (Fig. 2) may also be related to the phonon anharmonicity as well as the observed deviation of $\alpha_L(T)$ data from the Debye model.

Raman spectroscopic measurements for the $\text{Sb}_2\text{Te}_{3-x}\text{Se}_x$ ($0.2 \leq x \leq 1.0$) samples have been carried out between 80 and 300 K. The effect of defect concentration as well as Se doping on the Raman-active phonon modes of Sb_2Te_3 at room temperature was recently reported by us [7,35]. However, only limited effort is given in the temperature-dependent Raman spectroscopic study of Sb_2Te_3 and related systems [5,23,24]. In the synthesized $\text{Sb}_2\text{Te}_{3-x}\text{Se}_x$ samples, the same crystalline symmetry is maintained with Te replaced by isoelectronic Se in a stoichiometric amount [7]. For Sb_2Te_3 -based systems, group theory derives four Raman-active phonons at the centre of the Brillouin zone with wave vector $q = 0$ in the frequency range ~ 30 to 200 cm^{-1} : two degenerate E_g modes (E_g^1 and E_g^2) in which the atomic motion is perpendicular to the c axis (in-plane) and two nondegenerate A_{1g} (A_{1g}^1 and A_{1g}^2) modes with atomic motion directed along the c axis (out-of-plane) of the crystal [1,36,37]. First-principles calculation revealed the elemental contribution to the specific phonon modes, with the A_{1g}^1 mode corresponding to pure Te displacements and the A_{1g}^2 mode dominated by Sb displacements along the c axis [37]. For the present system under investigation, i.e., $\text{Sb}_2\text{Te}_{3-x}\text{Se}_x$ samples, Te atoms are replaced by Se and thus the variation of the A_{1g}^1 phonon mode, which corresponds to pure Te displacements, is of major interest. Hence, in order to find out the effect of Se doping on the vibrational phonon

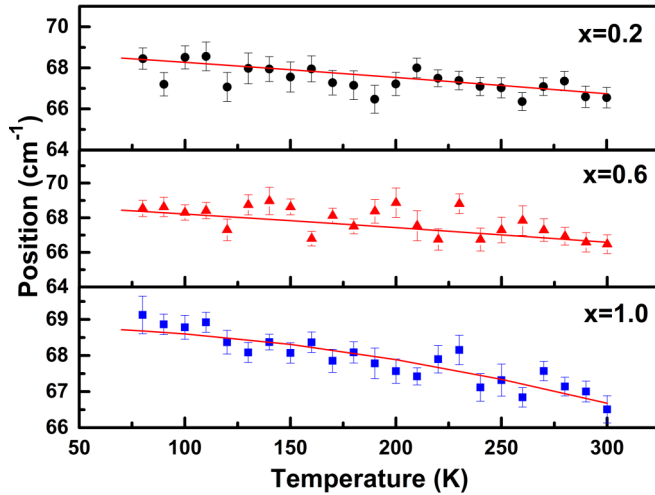


FIG. 6. Temperature dependence of the A_{1g}^1 phonon mode in $Sb_2Te_{3-x}Se_x$ ($0.2 \leq x \leq 1.0$) samples. The symbols represent peak positions extracted from the experimental data using Lorentzian peak fitting. The solid lines are best fit to the Klemens's model [Eq. (5)].

modes of the Sb_2Te_3 system, the temperature dependence of the A_{1g}^1 mode ($\sim 69 \text{ cm}^{-1}$) is investigated (Fig. 6).

Temperature-dependent Raman peak shifts of $Sb_2Te_{3-x}Se_x$ ($x = 0.2, 0.6$, and 1.0) samples are fitted with a symmetrical three-phonon coupling model (also known as Klemens's model) [38].

Phonon anharmonicity in Sb_2Te_3 , Bi_2Te_3 – based layered pnictide chalcogenides can be well described with this model [5,23,24]. It is considered that phonon-phonon coupling leads to the renormalization of phonon energy and lifetime. In the said model an optical phonon is assumed to decay into two phonons with equal energies and opposite momentum. Fitting with Klemens's model shows a good agreement with Raman peak shift and change in phonon lifetime, which enables us to extract the anharmonic contribution in lattice vibration of the $Sb_2Te_{3-x}Se_x$ system.

The extracted peak positions using Lorentzian fit for the $Sb_2Te_{3-x}Se_x$ ($0.2 \leq x \leq 1.0$) samples are shown in Fig. 6. Thermal variation of phonon frequency $\omega(T)$ is expressed as

$$\omega(T) = \omega_0 + \Delta\omega^{(1)}(T) + \Delta\omega^{(2)}(T), \quad (5)$$

where ω_0 is bare harmonic frequency, $\Delta\omega^{(1)}(T)$ is the anharmonic correction arising due to the lattice thermal expansion, and $\Delta\omega^{(2)}(T)$ is the anharmonic phonon-phonon coupling

term. The term $\Delta\omega^{(1)}(T)$ is given by

$$\Delta\omega^{(1)}(T) = \omega_0 \left[\exp\left(-\gamma_G \int_0^T [\alpha_{c_H}(T') + 2\alpha_{a_H}(T')] dT'\right) - 1 \right], \quad (6)$$

where the symbols have their usual meaning. The γ_G values of each Se-doped Sb_2Te_3 samples have already been estimated using Eq. (3). In addition, for verification, $\overline{\gamma_G}$ is estimated by the linear fit of $\ln[\omega(T)]$ vs $\ln[V(T)]$ graph and using the relation

$$\overline{\gamma_G} = -\partial \ln \omega / \partial \ln V, \quad (7)$$

where $V(T)$ [$V = (\sqrt{3}/2)a_H^2 c_H$] is the thermal variation of the unit-cell volume. The plots for $\overline{\gamma_G}$ are presented in Fig. SM2 of the Supplemental Material [13]. It is obtained that γ_G and estimated $\overline{\gamma_G}$ are the same. The anharmonic phonon-phonon coupling term is represented by

$$\Delta\omega^{(2)}(T) = A_1 [1 + n(\omega_1) + n(\omega_2)], \quad (8)$$

with $\omega_1 = \omega_2 = \omega_0/2$ and $n(\omega) = [\exp(h\omega/k_B T) - 1]^{-1}$, where A_1 is the fitting parameter. The theoretical fit to Klemens's model is displayed in Fig. 6 by the solid red line along with the experimental data of peak shift of the $Sb_2Te_{3-x}Se_x$ samples. The obtained best-fit values of A_1 are 0.010 ± 0.002 , 0.024 ± 0.002 , and 0.033 ± 0.002 for $x = 0.2$, 0.6 , and 1.0 , respectively. Thermal variation of the anharmonic terms $\Delta\omega^{(1)}(T)$ and $\Delta\omega^{(2)}(T)$, presented in Table II, depicts that anharmonic contributions increase with increasing temperature. Further attempt is made to model the temperature dependence of phonon linewidth $L(T)$ within the symmetrical three-phonon coupling approximation:

$$L(T) = A_2 [1 + n(\omega_1) + n(\omega_2)], \quad (9)$$

where A_2 is the fitting parameter and other symbols have their usual meaning. Phonon linewidth, a measure of phonon lifetime, is expressed in terms of anharmonic coupling only and does not depend on the thermal expansion contribution. The comparison between the calculated and the experimental $L(T)$ is shown in Fig. SM3 in the Supplemental Material [13]. The fitting parameter $A_2 = 1.14 \pm 0.05$ ($x = 0.2$), 1.54 ± 0.06 ($x = 0.6$), and 1.61 ± 0.07 ($x = 1.0$) extracted for the present $Sb_2Te_{3-x}Se_x$ ($0.2 \leq x \leq 1.0$) samples is in agreement with those reported for Sb_2Te_3 [23]. It is interesting to note that both A_1 and A_2 change in a similar fashion, i.e., increase with increasing Se(x) content in $Sb_2Te_{3-x}Se_x$ ternary mixed

TABLE II. Temperature dependence of anharmonic terms and as obtained for $Sb_2Te_{2.8}Se_{0.2}$, $Sb_2Te_{2.4}Se_{0.6}$, and Sb_2Te_2Se samples. Units are cm^{-1} .

T (K)	$Sb_2Te_{2.8}Se_{0.2}$		$Sb_2Te_{2.4}Se_{0.6}$		Sb_2Te_2Se	
	$\Delta\omega^{(1)}(T)$	$\Delta\omega^{(2)}(T)$	$\Delta\omega^{(1)}(T)$	$\Delta\omega^{(2)}(T)$	$\Delta\omega^{(1)}(T)$	$\Delta\omega^{(2)}(T)$
80	$0.57 \pm 1.4 \times 10^{-3}$	$0.03 \pm 0.8 \times 10^{-4}$	$0.64 \pm 1.6 \times 10^{-3}$	$0.08 \pm 2.0 \times 10^{-4}$	$0.23 \pm 0.6 \times 10^{-3}$	$0.11 \pm 2.8 \times 10^{-4}$
100	$0.72 \pm 1.8 \times 10^{-3}$	$0.04 \pm 1.0 \times 10^{-4}$	$0.81 \pm 2.0 \times 10^{-3}$	$0.10 \pm 2.5 \times 10^{-4}$	$0.34 \pm 0.9 \times 10^{-3}$	$0.13 \pm 3.3 \times 10^{-4}$
150	$1.10 \pm 2.7 \times 10^{-3}$	$0.06 \pm 1.5 \times 10^{-4}$	$1.25 \pm 3.1 \times 10^{-3}$	$0.15 \pm 3.8 \times 10^{-4}$	$0.69 \pm 1.7 \times 10^{-3}$	$0.19 \pm 4.8 \times 10^{-4}$
200	$1.49 \pm 3.7 \times 10^{-3}$	$0.08 \pm 2.0 \times 10^{-4}$	$1.69 \pm 4.2 \times 10^{-3}$	$0.20 \pm 5.0 \times 10^{-4}$	$1.19 \pm 2.9 \times 10^{-3}$	$0.27 \pm 6.8 \times 10^{-4}$
250	$1.90 \pm 4.7 \times 10^{-3}$	$0.10 \pm 2.5 \times 10^{-4}$	$2.16 \pm 5.4 \times 10^{-3}$	$0.24 \pm 6.0 \times 10^{-4}$	$1.79 \pm 4.4 \times 10^{-3}$	$0.33 \pm 8.3 \times 10^{-4}$
300	$2.32 \pm 5.8 \times 10^{-3}$	$0.12 \pm 3.0 \times 10^{-4}$	$2.64 \pm 6.6 \times 10^{-3}$	$0.29 \pm 7.3 \times 10^{-4}$	$2.53 \pm 6.3 \times 10^{-3}$	$0.40 \pm 10.0 \times 10^{-4}$

crystals, depicting that anharmonicity increases as a function of Se concentration.

Thermal variation of the Raman peak shows a redshift with increasing temperature [Fig. 6]. Yang *et al.* [39] explained the Raman shifts with bond-order-length strength and local bond-averaging approach. Thermal softening of the phonon mode strongly depends on the cohesive energy and θ_D of the material. It is noteworthy to mention that θ_D of the $\text{Sb}_2\text{Te}_{3-x}\text{Se}_x$ ($0.2 \leq x \leq 1.0$) samples increases with increasing Se(x) content (Table I). Thermal softening of the phonon mode occurs with increasing temperature due to the thermal lengthening as well as weakening of the involved bonds giving rise to the observed redshift of Raman peaks. Deviation of the measured C_p from the theoretical C_v value increases with increasing Se(x) content and corroborates the observed redshift of the phonon modes. The bare harmonic frequency (ω_0) in Klemens's model shows no significant variation with Se concentration, viz., 69.0 ± 0.2 , 68.9 ± 0.2 , and $68.8 \pm 0.2 \text{ cm}^{-1}$ for $x = 0.2, 0.6$, and 1.0 , respectively. The value of ω_0 is related to the second-order expansion of the lattice potential in normal coordinates. The anharmonic contribution in lattice thermal expansion as well as the phonon-phonon coupling term increases with temperature, as depicted by the thermal variation of $\Delta\omega^{(1)}(T)$ and $\Delta\omega^{(2)}(T)$ terms, respectively (Table II). Thermal expansion coefficient $\alpha_L(T)$ of the $\text{Sb}_2\text{Te}_{3-x}\text{Se}_x$ ($x = 0.2, 0.6$, and 1.0) samples, presented in Figs. 4 and 5, also indicates the presence of higher-order anharmonic contributions in lattice vibrations. It is noteworthy to mention that changes in $\Delta\omega^{(2)}(T)$ ($= [\Delta\omega^{(2)}(T)_{300 \text{ K}} - \Delta\omega^{(2)}(T)_{80 \text{ K}}] / [\Delta\omega^{(2)}(T)_{300 \text{ K}}] \times 100\%$) in the temperature range of 80 to 300 K are the same for all the Se-doped samples. However, changes in $\Delta\omega^{(1)}(T)$ between 80 and 300 K increase with increasing Se content. Hence, in order to confirm the effect of Se doping on $\Delta\omega^{(1)}(T)$ as well as point out the role of anharmonic lattice vibration in $\text{Sb}_2\text{Te}_{3-x}\text{Se}_x$ samples, we co-plotted percentage changes in $\Delta\omega^{(1)}(T)$ ($= [\Delta\omega^{(1)}(T)_{300 \text{ K}} - \Delta\omega^{(1)}(T)_{80 \text{ K}}] / [\Delta\omega^{(1)}(T)_{300 \text{ K}}] \times 100\%$) and γ_G with Se(x) in Fig. 7 and observed that they change in

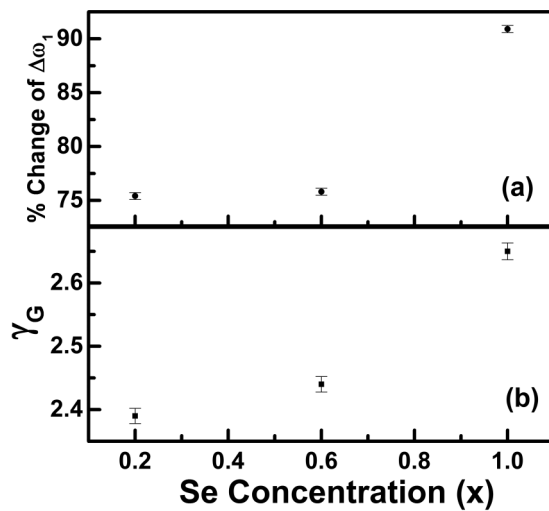


FIG. 7. Evolution of (a) percentage change of $\Delta\omega^{(1)}(T) = [\Delta\omega^{(1)}(T)_{300 \text{ K}} - \Delta\omega^{(1)}(T)_{80 \text{ K}}] / [\Delta\omega^{(1)}(T)_{300 \text{ K}}] \times 100\%$. (b) Grunisen parameter γ_G with varying Se(x) content.

TABLE III. Lattice thermal conductivity (κ_L) and velocity of sound (v_S) at 300 K, and best-fit values of parameter C [refer to Eq. (12)] for $\text{Sb}_2\text{Te}_{3-x}\text{Se}_x$ samples.

Sample	$\kappa_L (\text{Wm}^{-1} \text{K}^{-1})$	$v_S (\text{km/s})$	C parameter
0.2	3.02 ± 0.075	1.82	$4.82 \pm 6 \times 10^{-3}$
0.6	2.79 ± 0.069	1.83	$6.83 \pm 2 \times 10^{-3}$
1.0	0.75 ± 0.002	1.85	$7.08 \pm 1 \times 10^{-3}$

similar fashion. Thus, phonon anharmonicity increases with increasing Se(x) content and plays a significant role in the $\text{Sb}_2\text{Te}_{3-x}\text{Se}_x$ ($0.2 \leq x \leq 1.0$) system.

Recently Lee *et al.* [11] demonstrated that strong anharmonic scattering significantly affects κ_L in IV–VI compound-based TE materials like lead chalcogenides, SnTe, and others [11]. This prompts us to estimate the influence of phonon anharmonicity on κ_L of the present $\text{Sb}_2\text{Te}_{3-x}\text{Se}_x$ system. Not much effort is put forward in understanding the lattice dynamics, phonon anharmonicity, and its connection to κ_L of the Sb_2Te_3 -based system. κ_L is determined by various phonon-scattering mechanisms, viz., phonon-phonon interaction and defect scattering. The heat is conducted by acoustic phonons and at high temperature, the Umklapp process is dominant in scattering heat-conducting phonons [15]. It is noteworthy to mention that the phonon-phonon scattering in the Umklapp process is anharmonic in nature. An expression for κ_L in the Umklapp scattering limit, derived by Slack [40], is provided by Eq. (10):

$$\kappa_L = \Lambda \frac{\bar{M}\theta_D^3\delta}{\gamma_G^2 n^{2/3} T}, \quad (10)$$

where \bar{M} is the average atomic mass in the unit cell, δ^3 is the volume per atom, and n is the number of atoms in the primitive cell. $\text{Sb}_2\text{Te}_{3-x}\text{Se}_x$ has five atoms per primitive cell. Λ is a physical constant $\sim 3.1 \times 10^{-6}$ if κ_L is in W/mK, \bar{M} in amu, and δ in Å. Bessas *et al.* [1] and Zhang *et al.* [15] demonstrated that Eq. (10) generates reasonable values of κ_L for Sb_2Te_3 and lead chalcogenides, respectively. Using average atomic mass (\bar{M}), d^3 as obtained from Reitveld refinement and the estimated values of θ_D and γ_G, κ_L is calculated for the $\text{Sb}_2\text{Te}_{3-x}\text{Se}_x$ ($x = 0.2, 0.6$, and 1.0) samples and presented in Table III. It is depicted that κ_L decreases with increasing Se(x) concentration. In Fig. 8, variation of κ_L against γ_G and Se(x) is plotted, which clearly indicates that κ_L decreases with increasing anharmonicity (γ_G) as well as Se(x) content. Like IV–VI compounds, anharmonic scattering significantly influences κ_L in the Se-doped Sb_2Te_3 system and the value of κ_L decreases with increasing phonon anharmonicity.

It is noteworthy to mention that $\text{Sb}_2\text{Te}_{3-x}\text{Se}_x$ samples possess structural anisotropy, which increases with increasing temperature and Se content (Fig. 2). We attempt to find the correlation between structural anisotropy and phonon anharmonicity and provide a plausible explanation of increasing phonon anharmonicity with increasing Se content in $\text{Sb}_2\text{Te}_{3-x}\text{Se}_x$ ($0.2 \leq x \leq 1.0$) samples. The values of Debye-Waller factor (B_{iso}) for the $\text{Sb}_2\text{Te}_{3-x}\text{Se}_x$ ($x = 0.2, 0.6$, and 1.0) samples under investigation, as obtained from Rietveld refinement at different temperatures, is presented in the

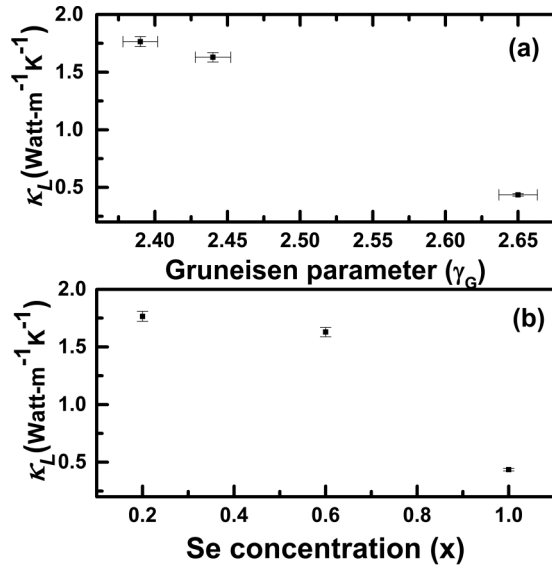


FIG. 8. Variation of estimated lattice thermal conductivity κ_L with (a) Gruneisen parameter (γ_G), and (b) Se concentration (x).

Supplemental Material [13]. B_{iso} , also known as atomic displacement parameter, is a measure of positional disorder, comprising both a static (B_{static}) and dynamic (B_{dynamic}) part [41,42]. For perovskite and multiferroic materials, comparable B_{iso} values have been obtained [41,43,44]. B_{static} , which is independent of temperature, can be calculated using the relation $B_{\text{static}} = 8\pi^2 \langle u_{\text{static}}^2 \rangle$, with $\langle u_{\text{static}}^2 \rangle = (r_A - r_B)^2 (x/3) [1 - (x/3)]$, where r_A ($= 1.4 \text{ \AA}$), r_B ($= 1.2 \text{ \AA}$) are atomic radii of Te and Se, respectively, and x ($= 0.2, 0.6$, and 1.0) is the concentration of solute atoms. Calculation yields $B_{\text{static}} = 0.2, 0.5$, and 0.7 \AA^2 , respectively. B_{dynamic} can be estimated easily using B_{static} and temperature-dependent B_{iso} values. B_{dynamic} is responsible for the temperature variation of B_{iso} values depicted in the Supplemental Material (Fig. SM1) [13]. The positional disorder arises due to the Se atom occupying an off-centered position in the rhombohedral lattice sites while replacing Te atoms. Such off-centering leads to the local distortion of average rhombohedral structure [42,45]. The presence of antisite defects and incorporation of Se in Sb_2Te_3 causes change in bond strength, bond length, and further distorts the local structure. The local structural distortion significantly affects the lattice vibration. The anharmonicity of phonon branches, which increases with increasing Se content, sets in with local structural distortion. In order to obtain further insight, thermal variation of θ_D for $\text{Sb}_2\text{Te}_{3-x}\text{Se}_x$ ($x = 0.2, 0.6$, and 1.0) samples is estimated using the relation [46]

$$B_{\text{iso}} = \left(\frac{6h^2}{Mk_B\theta_D} \right) \left[\frac{1}{4} + \left(\frac{T}{\theta_D} \right)^2 \int_0^{\theta_D/T} \frac{xdx}{e^x - 1} \right]. \quad (11)$$

Variation of θ_D with temperature, $\theta_D(T)$ of $\text{Sb}_2\text{Te}_{3-x}\text{Se}_x$ ($x = 0.2, 0.6$, and 1.0) samples, as evaluated from Eq. (11), is presented in Fig. 9. It is worth noting that the XRD data for $\text{Sb}_2\text{Te}_{2.8}\text{Se}_{0.2}$ were collected with an area detector and converted using IMAGEJ software, which may be the source of error giving rise to the observed fluctuations in the $\theta_D - T$ curve (Fig. 9) for this sample. Temperature variation of θ_D

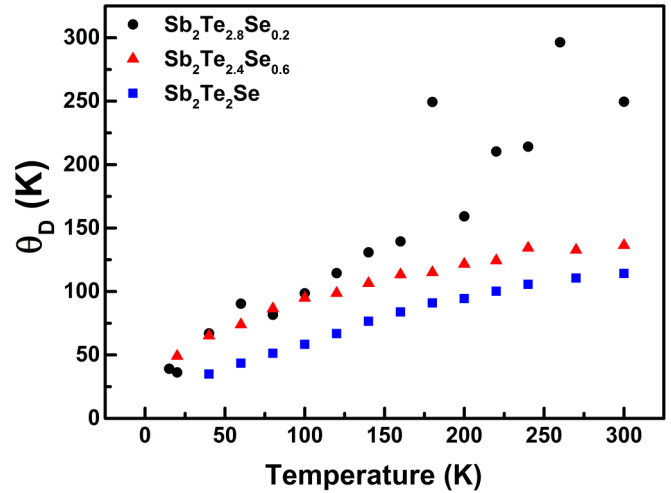


FIG. 9. Thermal variation of Debye temperature (θ_D) for the Se-doped Sb_2Te_3 samples. The errors in θ_D are within the size of the data points.

was reported earlier for Bi_2Se_3 and Bi_2Te_3 [14]. However, to date there is no such report for the Sb_2Te_3 -based layered chalcogenide system. The observed temperature dependence of θ_D is mostly due to the thermal variation of B_{dynamic} . In our recent paper, we demonstrated that positional disorder and change in bond strength leads to the increase of $\theta_D(T)$ with temperature in $\text{Bi}_{1-x}\text{Sb}_x$ ($0.10 \leq x \leq 0.20$) alloy [42]. However, Zhang *et al.* [15] reported temperature-dependent θ_D for the PbS system, which is manifested in strong deviation of the phonon spectrum from the Debye model and corroborates our $\alpha_L(T)$ data. It is noteworthy to mention that, like $\theta_D(T)$ data [Fig. 9], structural anisotropy increases with increasing temperature [Fig. 2]. This further suggests that the observed phonon anharmonicity and structural anisotropy of Se-doped Sb_2Te_3 system are completely correlated.

In order to obtain further insight, we analyzed the speed of sound (v_s) in the present $\text{Sb}_2\text{Te}_{3-x}\text{Se}_x$ system. The v_s and C_p are constituents of κ and anharmonicity, respectively. The role of disorder and anharmonicity in κ has been studied and their correlation is important in understanding the phonon dynamics of a system [1,47]. In this paper, we have already established the role of anharmonicity in κ . In addition, an attempt is made to derive v_s in Se-doped Sb_2Te_3 -based layered chalcogenides. v_s is obtained using the relation [47]

$$v_s = \frac{k_B\theta_D}{[\hbar(6\pi^2n)^{1/3}]}, \quad (12)$$

where temperature-dependent values of θ_D are used. The density of atoms (n) for $\text{Sb}_2\text{Te}_{3-x}\text{Se}_x$ ($x = 0.2, 0.6$, and 1.0) samples are, respectively, 3.19×10^{22} , 3.26×10^{22} , and 3.32×10^{22} atoms/cm³. The v_s values thus extracted are in excellent agreement with the previously reported values (Table III). In addition, fractional variation of v_s , i.e., velocity shift $\delta v_s/v_s$, is calculated, which linearly decreases with increasing temperature (Fig. 10). Such linear decrease of $\delta v_s/v_s$ with increasing temperature is a measure of anharmonic coupling between the sound waves and thermally excited low-energy vibrations [48]. Further temperature-dependent

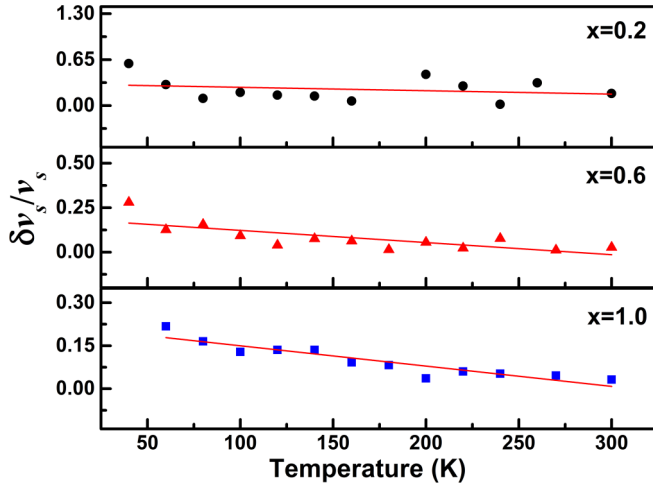


FIG. 10. Temperature-dependent variation of $\delta v_s/v_s$ for the $\text{Sb}_2\text{Te}_{3-x}\text{Se}_x$ ($x = 0.2, 0.6$, and 1.0) samples. A fit of the estimated data with Eq. (12) is represented by the red solid lines. The estimated errors in $\delta v_s/v_s$ are within the size of the data points.

variation of $\delta v_s/v_s$ is fitted with Eq. (13) [49]:

$$\frac{\delta v_s}{v_s} = -CT + D \ln \Omega, \quad (13)$$

where Ω is the ultrasonic angular frequency; C and D are constants. The first term (C) in Eq. (13) arises due to strong anharmonicity [48,49]. The fitted values of C increase with increasing Se content (Table III). It is thus quite justified to conclude that anharmonicity is indeed present in Se-doped Sb_2Te_3 samples and increases with increasing Se. First-principles studies suggest the resonant bonding mechanism is responsible for anharmonicity and our results are in accordance with the recent analysis of SnTe , PbTe , and SnSe thermoelectrics, where the authors revealed that strong anharmonicity leads to lower thermal conductivity [11,12]. The underlying anharmonicity stems from bonding instability arising due to long-range resonant p -bond network of Te/Se atoms. The long-ranged interaction cause softening of transverse optical (TO) phonons [11]. The softening of TO mode (E_g^2 phonon) is clearly evidenced in the synthesized $\text{Sb}_2\text{Te}_{3-x}\text{Se}_x$ ternary mixed crystals and is presented for a typical $x = 0.2$ sample in the Supplemental Material (Fig. SM4) [13]. The softening of TO mode reduced the phonon band gap and it is quite justified to assume that with increasing Se(x) content in the $\text{Sb}_2\text{Te}_{3-x}\text{Se}_x$ ($0.2 \leq x \leq 1.0$) system the phonon band gap decreases and more acoustic phonons get scattered by TO phonons. Only high-frequency acoustic phonons can participate in the scattering process when the gap is large. With a reduced gap most acoustic phonons, regardless of frequency, are scattered by optical phonons and the effective phonon scattering increases, leading toward lower κ values in high Se-doped samples. The observation corroborates our κ_L values estimated above, where it has been clearly demonstrated that κ_L decreases with increasing Se content (Fig. 8). However, we should mention that no data, to the best of our knowledge, relating the resonant bonding states in anharmonicity of Sb_2Te_3 -based system are readily

available for direct comparison. Thus, in order to further clarify the role of resonant Te/Se band in anharmonicity of the $\text{Sb}_2\text{Te}_{3-x}\text{Se}_x$ system, detailed theoretical and experimental study of single-crystal samples is needed. Very recently, Tian *et al.* [5] pointed out that apart from reducing κ , large anharmonicity also induces ferroelectricity and structural phase transition [10,50,51]. Our temperature-dependent synchrotron powder-diffraction study excludes the possibility of structural phase transition in Se-doped Sb_2Te_3 system, but confirms anharmonicity-induced lowering of thermal conductivity. Our results clearly demonstrate that anharmonicity engineering in the Sb_2Te_3 -based system represents a good opportunity for improving its thermoelectric performance and would help researchers to design better thermoelectric material.

IV. CONCLUSION

The phonon anharmonicity in lattice dynamics of polycrystalline $\text{Sb}_2\text{Te}_{3-x}\text{Se}_x$ ($x = 0.2, 0.6$, and 1.0)-based thermoelectric materials was investigated with temperature-dependent x-ray diffraction, Raman spectroscopic measurements, and heat-capacity study. The XRD data ruled out structural phase change in the measured temperature range (20 to 300 K). Both structural anisotropy and Debye temperature (θ_D) indicate similar temperature dependence. Linear thermal-expansion coefficients of all the $\text{Sb}_2\text{Te}_{3-x}\text{Se}_x$ ($0.2 \leq x \leq 1.0$) samples are extracted. The thermal-expansion coefficient values deviate from the Debye model due to the presence of higher-order anharmonic components. Around room temperature, substantial deviation of experimentally measured C_p values from Dulong-Petit law is observed. The deviation increases with increasing Se content and is attributed to phonon anharmonicity. The dimensionless Gruneisen parameter (γ_G) increases with increasing Se content. The temperature dependence of the A_{1g}^1 mode, responsible for pure Te displacement, is analyzed considering the symmetrical three-phonon coupling model (Klemens's model) and the material thermal expansion. The analysis revealed that anharmonicity is the key to explain the temperature-dependent phonon frequency shifts of the A_{1g}^1 mode for the Se-doped Sb_2Te_3 samples and the phonon anharmonicity arising due to lattice thermal-expansion increases with increasing Se content. In addition, the theoretical values of the lattice thermal conductivity (κ_L) of the $\text{Sb}_2\text{Te}_{3-x}\text{Se}_x$ are estimated in the Umklapp scattering limit, which decreases with increasing γ_G . Further, softening of transverse optical phonon mode (E_g^2 phonon) is observed. The result thus confirms that phonon anharmonicity increases with increasing Se content in the reported $\text{Sb}_2\text{Te}_{3-x}\text{Se}_x$ samples.

ACKNOWLEDGMENTS

The work is supported by DST, Government of India-RFBR, Government of Russia (DST Ref. No. INT/RUS/RFBR/P-183), and UGC DAE CSR, Kalpakkam node (Project Reference No. CSR-KN/CRS-65/2014-15/505). Two of the authors (D.D. and P.S.) are grateful to UGC DAE CSR, Kalpakkam node and DST, Government of India for providing financial assistance in the form of research fellowship through Project No. CSR-KN/CRS-65/2014-15/505 and

INT/RUS/RFBR/P-183, respectively. One of the authors (S.D.) is thankful to UGC, Government of India for providing him with a Junior Research Fellowship. The authors would also like to thank DST, Government of India, for the financial support

and SINP, India for facilitating the experiments at the Indian Beamline, Photon Factory, KEK, Japan. We are grateful to Dr. R. Rawat and P. Bag, UGC DAE CSR, Indore for heat capacity measurements.

-
- [1] D. Bessas, I. Sergueev, H.-C. Wille, J. Perßon, D. Ebling, and R. P. Hermann, *Phys. Rev. B* **86**, 224301 (2012).
- [2] H. Zhang, C.-X. Liu, X.-L. Qi, X. Dai, Z. Fang, and S.-C. Zhang, *Nat. Phys.* **5**, 438 (2009).
- [3] Y. Xia, D. Qian, D. Hsieh, L. Wray, A. Pal, H. Lin, A. Bansil, D. Grauer, Y. Hor, R. J. Cava *et al.*, *Nat. Phys.* **5**, 398 (2009).
- [4] I. Efthimiopoulos, J. Zhang, M. Kucway, C. Park, R. C. Ewing, and Y. Wang, *Sci. Rep.* **3**, 2665 (2013).
- [5] Y. Tian, S. Jia, R. J. Cava, R. Zhong, J. Schneeloch, G. Gu, and K. S. Burch, *Phys. Rev. B* **95**, 094104 (2017).
- [6] D. Biswas, S. Thakur, G. Balakrishnan, and K. Maiti, *Sci. Rep.* **5**, 17351 (2015).
- [7] D. Das, K. Malik, A. K. Deb, V. A. Kulbachinskii, V. G. Kytin, S. Chatterjee, D. Das, S. Dhara, S. Bandyopadhyay, and A. Banerjee, *Europhys. Lett.* **113**, 47004 (2016).
- [8] A. Soni, Z. Yanyuan, Y. Ligen, M. K. K. Aik, M. S. Dresselhaus, and Q. Xiong, *Nano Lett.* **12**, 1203 (2012).
- [9] A. Akrap, A. Ubaldini, E. Giannini, and L. Forro, *Europhys. Lett.* **107**, 57008 (2014).
- [10] C. W. Li, J. Ma, H. B. Cao, A. F. May, D. L. Abernathy, G. Ehlers, C. Hoffmann, X. Wang, T. Hong, A. Huq, O. Gourdon, and O. Delaire, *Phys. Rev. B* **90**, 214303 (2014).
- [11] S. Lee, K. Esfarjani, T. Luo, J. Zhou, Z. Tian, and G. Chen, *Nat. Commun.* **5**, 3525 (2014).
- [12] C. W. Li, J. Hong, A. F. May, D. Bansal, S. Chi, T. Hong, G. Ehlers, and O. Delaire, *Nat. Phys.* **11**, 1063 (2015).
- [13] See Supplemental Material at <http://link.aps.org/supplemental/10.1103/PhysRevB.96.064116> for the details of temperature dependent x-ray diffraction patterns after Rietveld refinement and the corresponding refinement parameters obtained using MAUD software, estimation of mode Grüneisen parameter, temperature dependence of phonon linewidth for the polycrystalline $\text{Sb}_2\text{Te}_{3-x}\text{Se}_x$ ($x = 0.2, 0.6, \text{ and } 1.0$) samples and temperature dependence of the E_g^2 phonon mode of a typical $\text{Sb}_2\text{Te}_{2.8}\text{Se}_{0.2}$ sample.
- [14] G. E. Shoemaker and J. A. Rayne, *Phys. Rev.* **185**, 1046 (1969).
- [15] Y. Zhang, X. Ke, C. Chen, J. Yang, and P. R. C. Kent, *Phys. Rev. B* **80**, 024304 (2009).
- [16] L. D. Zhao, S.-H. Lo, Y. Zhang, H. Sun, G. Tan, C. Uher, C. Wolverton, V. P. Dravid, and M. G. Kanatzidis, *Nature (London)* **508**, 373 (2014).
- [17] S. Sassi, C. Candolfi, J. B. Vaney, V. Ohorodniichuk, P. Masschelein, A. Dauscher, and B. Lenoir, *Appl. Phys. Lett.* **104**, 212105 (2014).
- [18] Y. Zhang, X. Ke, P. R. C. Kent, J. Yang, and C. Chen, *Phys. Rev. Lett.* **107**, 175503 (2011).
- [19] Y. Zhao, K. T. E. Chua, C. K. Gan, J. Zhang, B. Peng, Z. Peng, and Q. Xiong, *Phys. Rev. B* **84**, 205330 (2011).
- [20] W. K. Chong, G. Xing, Y. Liu, E. L. Gui, Q. Zhang, Q. Xiong, N. Mathews, C. K. Gan, and T. C. Sum, *Phys. Rev. B* **90**, 035208 (2014).
- [21] C. K. Gan, J. R. Soh, and Y. Liu, *Phys. Rev. B* **92**, 235202 (2015).
- [22] X. Chen, H. D. Zhou, A. Kiswandhi, I. Miotkowski, Y. P. Chen, P. A. Sharma, A. L. Lima Sharma, M. A. Hekmaty, D. Smirnov, and Z. Jiang, *Appl. Phys. Lett.* **99**, 261912 (2011).
- [23] Y. Kim, X. Chen, Z. Wang, J. Shi, I. Miotkowski, Y. P. Chen, P. A. Sharma, A. L. Lima Sharma, M. A. Hekmaty, Z. Jiang, and D. Smirnov, *Appl. Phys. Lett.* **100**, 071907 (2012).
- [24] Y. Tian, G. B. Osterhoudt, S. Jia, R. J. Cava, and K. S. Burch, *Appl. Phys. Lett.* **108**, 041911 (2016).
- [25] D. Das, K. Malik, A. K. Deb, S. Dhara, S. Bandyopadhyay, and A. Banerjee, *J. Appl. Phys.* **118**, 045102 (2015).
- [26] L. Lutterotti, S. Matthies, and H. R. Wenk, in *Proceedings of ICOTOM14*, edited by J. A. Spunar (National Research Council of Canada, Ottawa, 1999), p.1599; IUCr: Newsl. CPD **21**, 14 (1999).
- [27] A. Pashinkin, A. Malkova, and M. Mikhailova, *Russ. J. Phys. Chem. A* **82**, 1035 (2008).
- [28] N. W. Ashcroft and N. D. Mermin, *Solid State Physics* (Brooks/Cole, Pacific Grove, CA, 1976).
- [29] N. Sakai, T. Kajiwara, K. Takemura, S. Minomura, and Y. Fujii, *Solid State Commun.* **40**, 1045 (1981).
- [30] C. Kittel, *Introduction to Solid State Physics* (John Wiley & Sons, New York, 2005).
- [31] P. Dutta, D. Bhoi, A. Midya, N. Khan, P. Mandal, S. S. Samatham, and V. Ganesan, *Appl. Phys. Lett.* **100**, 251912 (2012).
- [32] R. Felten, F. Steglich, G. Weber, H. Rietschel, F. Gompf, B. Renker, and J. Beuers, *Europhys. Lett.* **2**, 323 (1986).
- [33] J. W. Gardner and A. C. Anderson, *Phys. Rev. B* **23**, 474 (1981).
- [34] M. Saint-Paul, J. C. Lasjaunias, and M. Locatelli, *J. Phys. C* **15**, 2375 (1982).
- [35] D. Das, K. Malik, S. Bandyopadhyay, D. Das, S. Chatterjee, and A. Banerjee, *Appl. Phys. Lett.* **105**, 082105 (2014).
- [36] J. Secor, M. A. Harris, L. Zhao, H. Deng, S. Raoux, and L. Krusin-Elbaum, *Appl. Phys. Lett.* **104**, 221908 (2014).
- [37] G. C. Sosso, S. Caravati, and M. Bernasconi, *J. Phys.: Condens. Mater* **21**, 095410 (2009).
- [38] P. G. Klemens, *Phys. Rev.* **148**, 845 (1966).
- [39] X. X. Yang, Z. F. Zhou, Y. Wang, R. Jiang, W. T. Zheng, and C. Q. Sun, *J. Appl. Phys.* **112**, 083508 (2012).
- [40] G. A. Slack, *Solid State Phys.* **34**, 1 (1979).
- [41] A. Singh, C. Moriyoshi, Y. Kuroiwa, and D. Pandey, *Phys. Rev. B* **88**, 024113 (2013).
- [42] K. Malik, D. Das, A. K. Deb, V. A. Kulbachinskii, V. Srihari, S. Bandyopadhyay, and A. Banerjee, *Europhys. Lett.* **115**, 58001 (2016).
- [43] C. Malibert, B. Dkhil, J. M. Kiat, D. Dutrand, J. F. Berar, and A. S. Bire, *J. Phys.: Condens. Matter* **9**, 7485 (2000).
- [44] R. R. Ragini, S. K. Mishra, and D. Pandey, *J. Appl. Phys.* **92**, 3266 (2002).
- [45] A. Singh, V. Pandey, R. K. Kotnala, and D. Pandey, *Phys. Rev. Lett.* **101**, 247602 (2008).

- [46] P. Fischer, I. Sosnowska, and M. Szymanski, *J. Phys. C: Solid State Phys.* **11**, 1043 (1978).
- [47] R. P. Hermann, F. Grandjean, and G. J. Long, *Am. J. Phys.* **73**, 110 (2005).
- [48] R. Nava, *Phys. Rev. B* **49**, 4295 (1994).
- [49] G. Bellessa, *Phys. Rev. Lett.* **40**, 1456 (1978).
- [50] I. Katayama, H. Aoki, J. Takeda, H. Shimosato, M. Ashida, R. Kinjo, I. Kawayama, M. Tonouchi, M. Nagai, and K. Tanaka, *Phys. Rev. Lett.* **108**, 097401 (2012).
- [51] K. Fujii, Y. Aikawa, and K. Ohoka, *Phys. Rev. B* **63**, 104107 (2001).